CERN-SPSC-2006-007
SPSC-SR-003
30th January 2006

Memorandum to the SPSC

Status Report of the ATHENA Collaboration

M. Amoretti[*], C. Amsler[†], G. Bonomi[**], P. D. Bowe[‡], C. Canali[*,§], C. Carraro[*,§], C. L. Cesar,[¶], M. Charlton[‖], M. Doser[**], A. Fontana[††,‡‡], M. C. Fujiwara[§§,¶¶], R. Funakoshi[¶¶], P. Genova[††,‡‡], J. S. Hangst[‡], R. S. Hayano[¶¶], L. V. Jørgensen[‖], A. Kellerbauer[**], V. Lagomarsino[*,§], R. Landua[**], E. Lodi Rizzini[‡‡,***], M. Macrí [*], N. Madsen[‡], G. Manuzio[*,§], P. Montagna[††,‡‡], L. G. Posada[¶¶], H. Pruys[†], C. Regenfus[†], A. Rotondi[††,‡‡], D. Mitchard[‖], G. Testera[*,§], A. Variola[*], L. Venturelli[‡‡,***], Y. Yamazaki[§§,†††], D. P. van der Werf[‖] and N. Zurlo[‡‡,***]

[*] *Istituto Nazionale di Fisica Nucleare, Sezione di Genova, 16146 Genova, Italy*
[†] *Physik-Institut, Zürich University, CH-8057 Zürich, Swtzerland*
[**] *PH Department, CERN, 1211 Geneva 23, Switzerland*
[‡] *Department of Physics and Astronomy, University of Aarhus, 8000 Aarhus C, Denmark*
[§] *Dipartimento di Fisica, Università di Genova, 16146 Genova, Italy*
[¶] *Instituto de Fisica, Universidade Federal do Rio de Janeiro, Rio de Janeiro 21945-970, Brazil*
[‖] *Department of Physics, University of Wales Swansea, Swansea SA2 8PP, UK*
[††] *Dipartimento di Fisica Nucleare e Teorica, Università di Pavia, 27100 Pavia, Italy*
[‡‡] *Istituto Nazionale di Fisica Nucleare, Sezione di Pavia, 27100 Pavia, Italy*
[§§] *Atomic Physics Laboratory, RIKEN, Saitama 351-0198, Japan*
[¶¶] *Department of Physics, University of Tokyo, Tokyo 113-0033, Japan*
[***] *Dipartimento di Chimica e Fisica per l'Ingegneria e per i Materiali, Università di Brescia, 25123 Brescia, Italy*
[†††] *Graduate School of Arts and Sciences, University of Tokyo, Tokyo, 153-8902, Japan*

Abstract. The ATHENA/AD-1 experiment at CERN produced for the first time in 2002 cold antihydrogen atoms by mixing of antiprotons and a positron plasma. The more relevant results obtained in the last three years are presented and discussed in the light of the antihydrogen formation processes. Emphasis is put on the results of the last year.

Keywords: Antihydrogen; Recombination; Penning trap; Positron plasma; Antiprotons
PACS: 36.10.-k

1. INTRODUCTION

Antihydrogen physics started in 1996 when the PS210 experiment at CERN reported the production of the first 9 atoms of antihydrogen [1]. Soon after the E862 experiment at Fermilab confirmed, with another 100 antiatoms, that the creation of antihydrogen was possible [2]. Both of these experiments generated in-flight antiatoms with a very low efficiency and at high energies, rendering practically impossible any further atomic

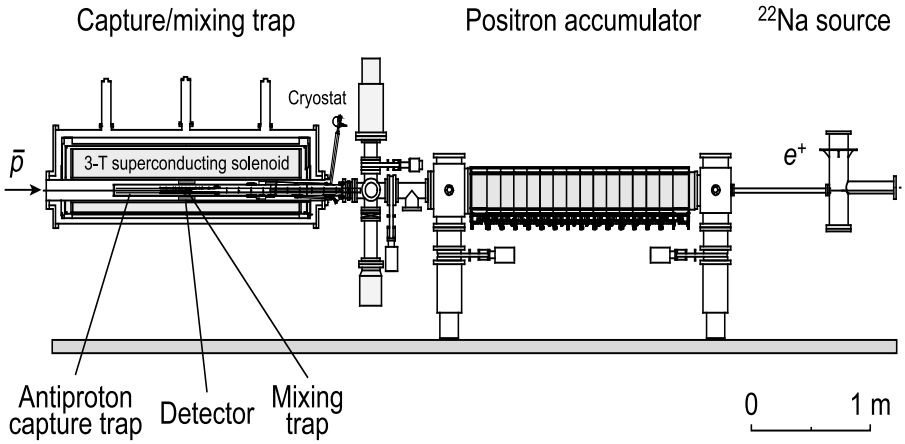

Figure 1. Overview of the ATHENA apparatus. Shown on the left is the superconducting 3-T solenoid magnet which houses the capture trap, the mixing trap, and the antihydrogen annihilation detector. On the right, the radioactive sodium source for positron production and the 0.14-T positron accumulation Penning trap.

physics study. In 2002 the next generation experiments at CERN, first ATHENA [3] and then ATRAP [4], reported the production of cold antihydrogen by mixing antiprotons ($\overline{p}$ s) and positrons at low temperature in a nested Penning trap [5].

After three years of running, ATHENA finished data taking in 2004. In this report we recall the main results obtained in this period, with emphasis on the work of the last year, that includes also the analysis of the 2004 data.

In the future the creation of a sample of trapped and laser cooled antihydrogen ($\overline{H}$) atoms to temperatures in the mK range will be a huge step toward a class of entirely new and crucial experiments on antihydrogen spectroscopy and antimatter gravity tests.

The ATHENA apparatus [6] (see Fig. 1) used antiprotons delivered by CERN's Antiproton Decelerator (AD) and positrons emitted from a ^{22}Na radioactive source (1.4×10^9 Bq). Both the $\overline{p}$ s and the positrons were trapped, cooled and accumulated in separate traps prior to moving and mixing in a common trap (called the *mixing* trap) in the central region. The positron accumulation trap was located inside a room temperature vacuum chamber in a 0.14 T magnetic field. The antiproton capture trap and the mixing trap were located in the 3 T field of a superconducting magnet whose bore was kept at 130 K under normal operation. A liquid-helium cryostat reduced the temperature of the trap region to about 15 K. Ultra-high vacuum conditions were also provided. The 3 Tesla solenoidal magnetic field provided the radial confinement and also allowed positrons to cool efficiently (with a time constant $\tau \simeq 0.5$ sec) to the trap temperature by the emission of synchrotron radiation.

When formed inside the mixing trap, neutral $\overline{H}$ atoms surviving collisions and field ionization escape the confinement region and annihilate on the trap electrodes producing a signal in the surrounding vertex detector [7] that triggers the detector readout (efficiency of 85 ± 10 %). The decay products of the annihilations (charged πs from the $\overline{p}$, γs from the e^+) are then reconstructed, making possible the three-dimensional imaging of antiproton and positron annihilations in the Penning trap [8, 9].

Table 1. $\overline{H}$ production from the cold mixing cycles. The uncertainty on the number of produced $\overline{H}$ and injected $\overline{p}$ is $\pm 5\%$.

	Long Cold Mix	Short Cold Mix
# of cycles	341	416
cycle duration (s)	180	70
total mixing time (s)	61 380	29 100
injected $\overline{p}$	2 924 000	5 065 000
produced $\overline{H}$	494 000	759 000
$\overline{H}$ production per cycle	$1\,450 \pm 80$	$1\,820 \pm 90$
$\overline{H}$ production rate (Hz)	8.0 ± 0.4	26.0 ± 1.3
$\overline{p}$ background (%)	35 ± 5	20 ± 3
$\overline{H}$ production per injected (%) $\overline{p}$	17 ± 2	15 ± 2

2. ANTIHYDROGEN PRODUCTION AND BACKGROUND IDENTIFICATION

In 2002-2003 ATHENA studied $\overline{H}$ formation in different mixing cycles, by varying the cycle duration and the positron plasma temperature.

In the “standard mixing cycle" the mixing trap is configured as a nested Penning trap [5], a configuration that allows simultaneous trapping of oppositely charged particles. The central part of the trap is then filled with about 3-7 $\times$ 10^7 e^+s. Once the positrons have self-cooled by synchrotron radiation, about 10^4 $\overline{p}$ s are injected and the two particle species interact for about 1-3 minutes. At the start of each mixing cycle the antiprotons are cooled by their passage through the positron plasma, and after few tens of ms antihydrogen formation begins [15, 11]. At the end of the mixing cycle the nested trap is emptied and both the number of positrons and antiprotons are counted before the process is restarted.

In the cold mixing cycle, when the positron temperature was that of the trap at 15 K, most of the annihilations took place on the trap electrodes because $\overline{H}$, being neutral, flew out and annihilated on the trap walls; the background was due to a small fraction of antiprotons annihilating in the trap center on rest gas atoms or ions.

In the hot mixing cycle, when the positron plasma is heated up to 8000 K, by exciting its axial dipole resonance (around 20 MHz), only the background events are observed [11, 12, 13]. The detector allows the different events to be fully identified and disentangled. The method is based mainly on the fit of some expected signal plus background distributions to the observations [8]. Two of these distributions, the vertex radial density and the opening angle cosine, are shown in fig 2.

The radial density represents the antiproton annihilation vertex position as reconstructed by the hits of the charged mesons in the two silicon strip layers of the detector. The profile of the hot mixing distribution (shaded histogram) shows clearly the presence of annihilations in the volume occupied by the positron potential well, where positive ions of the residual gas are trapped. The nature of this background has been extensively studied in the last year (see sect. 4.3).

The cosine of the opening angle distribution represents $\theta_{\gamma\gamma}$ of the two 511-keV γ rays recorded in time coincidence with the charged-particle hits, as seen from the charged-

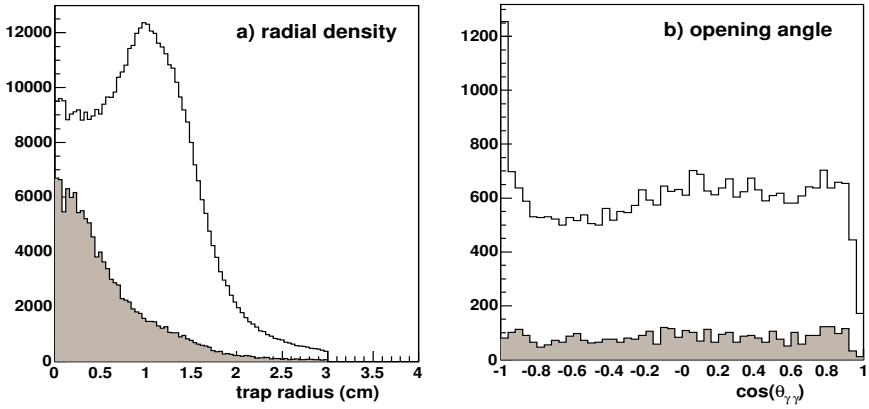

Figure 2. 2003 data. (a) Charged-meson vertex distribution as a function of the trap radius; (b) Opening-angle distribution of the photons recorded in coincidence with the charged-particle hits, as seen from the meson vertex. The shaded histograms refer to the background measured during the hot mixing cycles. The vertices are reconstructed with resolution σ_z=1.8 mm and $\sigma_x = \sigma_y$=3.5 mm. All the histograms are normalized to the number of antiprotons used in the cold mixing cycles.

particle vertex. The clear excess at $\cos(\theta_{\gamma\gamma}) = -1$ (corresponding to a back-to-back emission of the two γs typical of the $e^+ - e^-$ annihilation) is a proof of the presence of antihydrogen [3, 8]. It is also important to note that the flat part of the distribution contains antihydrogen signal, in the cases in which the detector or the reconstruction software were inefficient in the detection of both 511-keV γs. This inefficiency is mainly due to the presence of many low energy γs coming from the e.m. showers generated from the π^0 decay high energy γs in the magnet coils. As the MC calculations have shown [6, 8], the possibility to still extract a clear $\cos(\theta_{\gamma\gamma}) = -1$ peak in these highly unfavorable conditions comes from the high granularity of our crystal detector.

The $\overline{H}$ production for two different mixing times is shown in Tab. 1; these data represent the best results obtained so far for $\overline{H}$ production with a nested Penning trap.

We see that the shorter cycle data decreases the $\overline{p}$ background from 35% to about 20%, with only a small decrease of the yield per injected antiproton (from 17% to $\simeq$ 15%).

3. RESULTS 2002-2004

Here we recall briefly the results already reported extensively in our previous 2004 Report [10].

After having found the optimum conditions to proceed routinely, in 2003 ATHENA studied systematically the dependence of the antihydrogen production on the temperature and on the shape of the positron plasma [11, 12, 13, 14].

In [15] the time evolution of the cooling process was studied in detail. The existence of promptly produced antiatoms resulting from antiprotons that radially overlap with the positron cloud and quickly recombine ($t \simeq 10$ ms) has been shown, together with the presence of antiprotons that cool more slowly and represent a source of $\overline{H}$ for tens of

seconds.

In [11] we measured, for the first time, $\overline{H}$ production as a function of the positron plasma temperature from 15 K up to more than 3000 K.

The antihydrogen production is observed to decrease with increased positron plasma temperature, as expected (this effect was used in previous work to suppress the antihydrogen formation [3]), but the fall-off in antihydrogen production is slow enough that when the positron plasma is at room temperature the rate is still 1/3 of that observed in standard cold mixing conditions (15 K).

These results should be analyzed in terms of the two main processes that are involved in the $\overline{H}$ formation: the *two-body radiative capture* ($e^+ + \overline{p} \rightarrow \overline{H} + \gamma$) and the *three-body combination* ($e^+ + e^+ + \overline{p} \rightarrow \overline{H} + e^+$) [16]. The first process is the inverse of the photoelectric effect, the second one is the inverse of the ionization by collision and strongly depends on the plasma conditions and on the trap dynamics.

However, all attempts to fit the data with combinations of power laws, e.g. representing a mixture of two- and three-body processes, are unsuccessful. The naive scaling for the three-body reaction, $T^{-9/2}$, is clearly inconsistent with our data. It should be noted that collisional relaxation and finite transit time of the antiprotons through the positron plasma can lead to a different temperature scaling for the three-body reaction [17, 18, 19].

Following simple assumptions, the peak trigger rate, defined as the maximum value of the detector trigger rate after the start of mixing, should be comparable to the rate due to the radiative combination; given a temperature of 15 K, and assuming complete overlap between the two particle clouds, we calculated an antihydrogen production rate of about 40 Hz for 10000 $\bar{p}$s and 1.7×10^8 cm^{-3} positron plasma density. If we compare this value with our measured value of 432 ± 44 Hz [11] we clearly see that the experimental result is one order of magnitude higher. In other words the absolute measured production rate is not obviously compatible with a simple radiative calculation.

On the other hand, the three-body capture is a multi-step process depending on the trap dynamics and on the plasma characteristics, so that detailed predictions require specific Monte Carlo calculations. One of these simulations has recently considered the antihydrogen formation in a Penning trap, assuming the ATHENA positron plasma density and geometry [17]. The simulation finds that the $\overline{H}$ atoms that survive trap electrodes and e^+ plasma fields and annihilate on the trap walls have a binding energy greater than 40 K ($\simeq 3.5$ meV). Although no $\overline{H}$ production rate is calculated, there is a qualitative agreement between some predictions of this model and the ATHENA results: the antiatom yield is predicted to be around 33% to be compared to the observed one of 15-17% [8] (see also tab. 1), and a large fraction of antiatoms have greater than thermal velocity.

This last fact is in agreement with an analysis that we recently reported in [20], where, using the antihydrogen annihilation detector, experimental evidence that the spatial distribution of the emerging antihydrogen atoms is independent of the positron temperature and axially enhanced was obtained. Indeed, Fig. 3 [20] shows the axial distribution for $\overline{H}$ annihilations on the walls for cold mixing and for measurements with the e^+ plasma heated by 175 K and 500 K. There is no change in the shape of the distribution as a function of e^+ temperature, although the total number of events varies

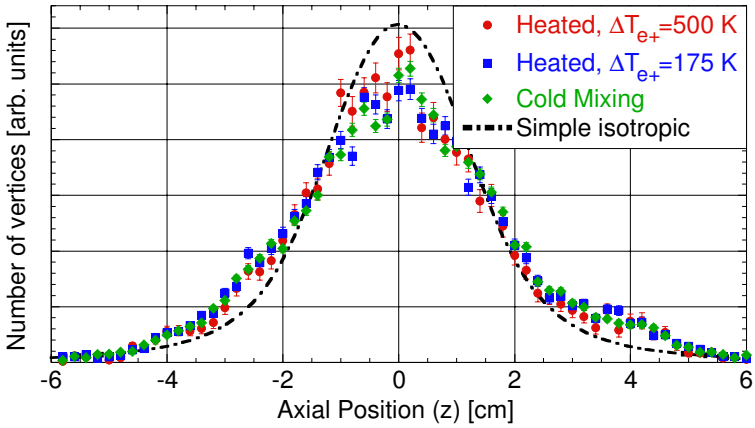

Figure 3. (Color online) Axial $\overline{H}$ distributions for cold mixing and mixing with e^+ heated by two different amounts (hot mixing subtracted). The dot-dashed line is a simple calculation of isotropic emission from the e^+ plasma volume. The distributions have been normalized to the same area.

strongly [3, 8]. Also shown in Fig. 3 is a simple calculation of the z-distribution resulting from isotropic emission of $\overline{H}$ from the ellipsoidal positron plasma.

We model our axial annihilation vertex distribution by randomly distributing $\overline{H}$ in a selected formation volume and assigning to each $\overline{H}$ a velocity from a three dimensional Gaussian velocity distribution characterized by transverse ($T_{\bar{p}}^{\perp}$) and axial ($T_{\bar{p}}^{||}$) temperatures and an azimuthal velocity given by the radial position of the $\overline{H}$. We use two different temperatures to describe non-equilibrium conditions. The intersection of the $\overline{H}$ undisturbed path with the cylindrical electrodes is then calculated. Then the vertex reconstruction resolution of the detector ($\sigma = 4$ mm), as well as the response function are folded onto the result. The $\bar{p}$ will, due to their mass, dominate the momentum of the $\overline{H}$ and we therefore neglect T_{e^+} in this model.

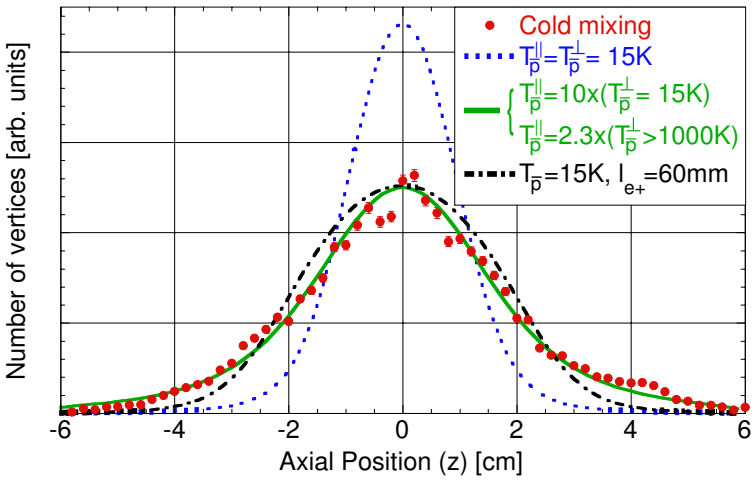

Figure 4. (Color online) Comparison of the axial distribution from cold mixing with a number of calculated distributions. Standard e^+ plasma parameters and $\mathbf{E} \times \mathbf{B}$ rotation were used except for the dot-dashed curve where $l_{e^+} = 60$ mm. Homogeneous formation in the plasma was assumed.

Fig. 4 shows a number of calculated distributions using the model described above. Also shown is the measured cold mixing distribution. The model does not reproduce the observations with $T_{\bar{p}}^{||} = T_{\bar{p}}^{\perp}$. A longer e^+ plasma gives a wider distribution, but the necessary length ($\sim$ 60 mm) to match the observed distribution is much larger than that measured. If we assume $T_{\bar{p}}^{\perp}$ = 15 K, the model matches the observed cold mixing distribution with $T_{\bar{p}}^{||} = (10 \pm 2) \times T_{\bar{p}}^{\perp}$ (solid curve in Fig. 4). This gives a lower limit of $T_{\bar{p}}^{||} = 150$ K.

The $\bar{p}$ which form $\overline{H}$ are therefore not in thermal equilibrium with the e^+. We cannot determine $T_{\bar{p}}$ of the $\bar{p}$ that form $\overline{H}$ from these measurements. However, as we increase $T_{\bar{p}}^{\perp}$ the necessary difference between the $T_{\bar{p}}^{||}$ and $T_{\bar{p}}^{\perp}$ to model the observations decreases asymptotically to a factor 2.3$\pm$0.6 (shown in Fig. 4). This is because the influence of $\mathbf{E} \times \mathbf{B}$ rotation on the distribution decreases with increasing temperature. Thus, even with no influence from $\mathbf{E} \times \mathbf{B}$ rotation we cannot find consistency with thermal equilibrium, i.e. our conclusion is independent of the absolute e^+ temperature.

In spite of these first analyses, a lot of further theoretical work is needed to clarify many questions concerning the production mechanisms, rates, temperature dependence and the final state distribution of the antihydrogen atoms produced. Due to the complexity of the problem, a complete simulation taking into account the three-body reaction, spontaneous radiative recombination, collisional excitation and de-excitation, radiative de-excitations and ionization of the formed atoms, giving predictions to be compared with our results, is still missing.

4. DATA ANALYSIS PERFORMED IN 2005

4.1. Radial centering of antiprotons

As has been discussed in the previous section, the anisotropy in the distribution of antihydrogen emission suggests that, when using the nested-well technique [5], in which hot antiprotons are launched into a positron plasma at liquid-helium temperature or slightly above, the temperature of the produced antihydrogen is several times higher than that of the positrons. Even if that were not the case, the cooled $\overline{p}$ would still be subject to the rigid rotation of the positron plasma, *i.e.*, the antiproton temperature is defined in the frame of the rotating plasma. The final antiproton deceleration stage, a degrader foil, leaves the captured $\overline{p}$ with large initial radial amplitudes. While the axial and modified cyclotron motions are quickly damped through collisions with electrons, the large magnetron radii of the confined antiprotons are retained throughout the entire stacking and transfer procedures. In addition to reducing the transfer efficiency between the capture region and the mixing trap, this may add a significant azimuthal component to the velocity of the produced antihydrogen. For this reason, we have extended a technique which is routinely used on heavy ions in buffer-gas-filled traps and applied it to antiprotons in order to center their radial motions prior to recombination [22].

The two independent radial motions carried out by charged particles in a Penning trap, the magnetron motion and the modified cyclotron motion, can be resonantly excited

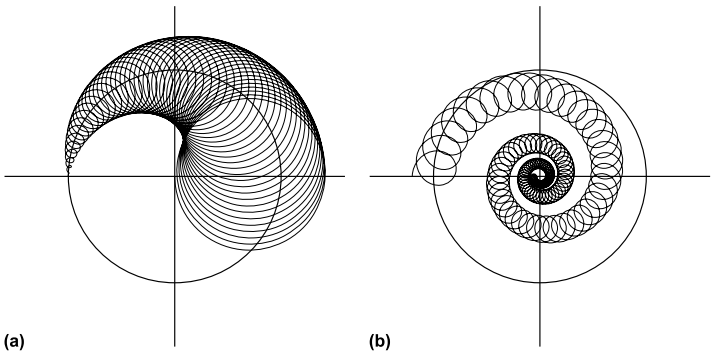

Figure 5. Azimuthal projection of the trajectory of an ion in a Penning trap under the influence of a quadrupolar excitation at the cyclotron frequency. (a) In the absence of a damping mechanism, the radial motions are continually converted into each other (for clarity, only one half of a full conversion is shown). (b) With damping, the radii of both modes are decreased and the ion is centered.

by azimuthal radio-frequency electric fields [23]. Quadrupolar excitation at the sum frequency of the two modes, the true cyclotron frequency $f_c = qB/(2\pi m)$, where q and m are the charge and mass of the particle and B is the magnetic-field magnitude, leads to a coupling between them which transfers the kinetic energy from one motion to the other and back, as shown in Fig. 5(a). In the presence of a cooling mechanism [24], the modified cyclotron motion is quickly damped and the total radial motion is centered [Fig. 5(b)]. Due to the fact that antiprotons would annihilate with a neutral atomic buffer gas, this damping must be supplied by sympathetic cooling with electrons which are simultaneously confined in the trap. The much lighter electrons have a much higher cyclotron frequency than the antiprotons and emit the absorbed energy via synchrotron radiation.

The measurements were performed in a small potential well near the center of the capture trap, shown in Fig. 6(a). In preparation for antiproton capture, electrons were preloaded into the capture trap from an electron source installed about 2 m downstream. After the capture and cooling of about 10^4 antiprotons in an electron plasma containing about 3×10^8 electrons at a density of about 10^8 cm^{-3}, some or all of the electrons were ejected from the potential well by applying short electric pulses to a neighboring electrode, leaving the 2000 times heavier antiprotons practically unaffected. A digital signal processor was then used to generate an RF signal at or near the cyclotron frequency of the $\overline{p}$ (about 45 MHz) with amplitude U_q and duration T_q, which was applied to the four-fold split electrode for the azimuthal excitation.

Despite the fact that a conversion of radial motions can never lead to a larger radial amplitude than the initial one, and thus radial loss, a shortfall of antiprotons in the final dump was observed after an excitation at the cyclotron frequency. This effect is probably due to magnetic-field inhomogeneities, which can exert a non-negligible force on the magnetic moments of the excited antiprotons. As can be seen from Fig. 6(b), the magnetic-field gradient is maximal near the electrode at which the $\overline{p}$ are confined, and the magnetic force counteracts the electric force applied during the final dump. An imperfection of the experimental apparatus thus allowed a convenient diagnosis of

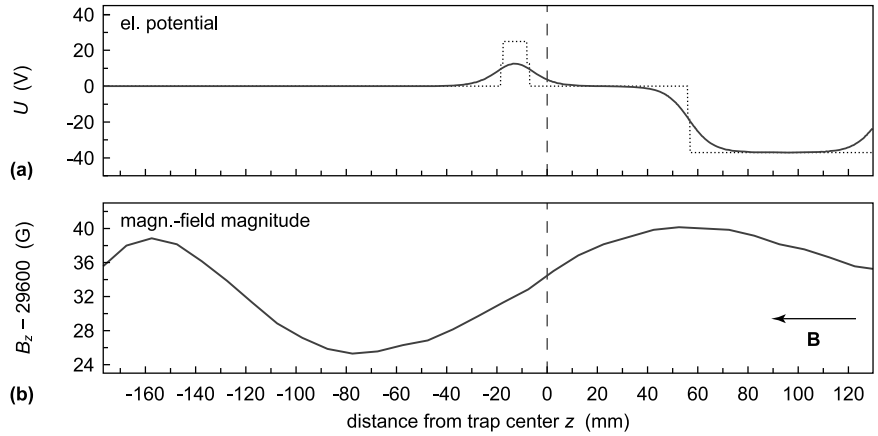

Figure 6. (a) Electric DC potential applied to the trap electrodes during sideband excitation. (b) Magnetic-field magnitude on the trap axis, measured with a Hall probe. The antiprotons are captured from the left and also dumped in the same direction.

successful conversion of the antiprotons' radial motions.

A quadrupolar excitation at the cyclotron frequency with varying amplitudes and/or durations was then applied, first in the absence, then in the presence of an electron buffer gas (about 1–3 × 10^6 e^-). Figures 7(a) and (b) show the disappearance of $\overline{p}$ as a function of the applied coupling strength $U_q T_q$ without and with damping, respectively. While in vacuum it was possible to map out several conversions from magnetron motion to modified cyclotron motion and back, the maximum available coupling strength was not sufficient to achieve complete conversion back to magnetron motion when electrons were present. Due to the shielding of the exciting field by the electron plasma, the conversion requires a roughly three times higher coupling strength.

As mentioned above, sideband cooling required both the conversion of radial modes and the damping of the modified cyclotron motion. In order to demonstrate the latter, we

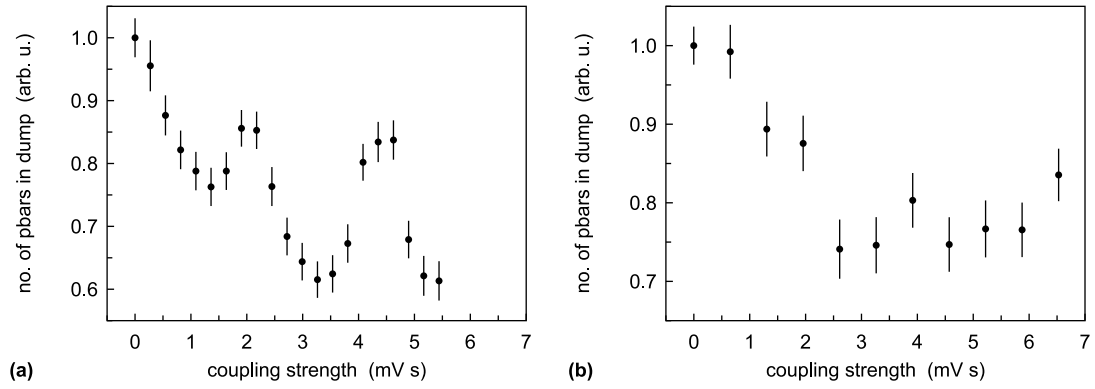

Figure 7. Number of antiprotons observed in the dump as a function of the coupling strength $U_q T_q$ of the quadrupolar excitation. (a) Without buffer gas, (b) with electron buffer gas.

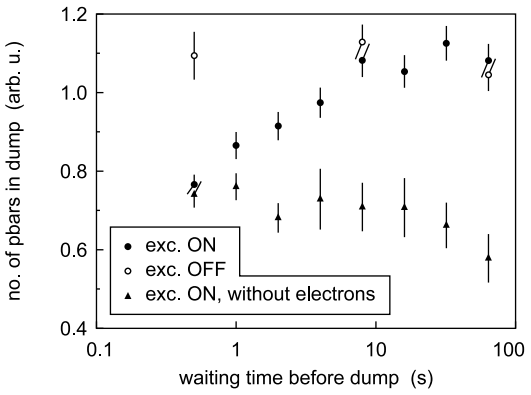

Figure 8. Cooling of the modified cyclotron motion. Antiprotons missing from a dump immediately after the quadrupolar excitation are recovered after a sufficiently long waiting time. The data points taken in the absence of electrons show that the excited antiprotons are not cooled and therefore not recovered in the dump even after waiting times of many tens of seconds.

performed a measurement of the number of antiprotons observed in the final dump as a function of the waiting time after having applied a full conversion. Figure 8 shows that the $\overline{p}$ which are absent from the dump if it takes place immediately after the excitation reappear after a sufficient waiting time. The figure confirms that the particles were not actually lost, but still present within the trap, thereby supporting our hypothesis for the disappearance mechanism. From the first few data points of the graph, a cooling time constant of the modified cyclotron motion of about 5 s can be inferred. Furthermore, the figure shows that in the absence of the electron buffer gas, the antiprotons whose motions have been converted are not recovered, even after very long waiting times.

While the results presented here do not provide a quantitative measure of the reduction of the $\overline{p}$'s radial amplitudes, they are consistent with antiproton centering. If the scheme can be successfully incorporated into the antihydrogen production cycle of a future experiment, it will not only allow the production of $\overline{H}$ as cold as the surrounding trap, but also increase the production rate due to better overlap between $\overline{p}$ and e^+, as well as improve the overlap with laser beams for stimulated recombination, laser cooling, or spectroscopy experiments.

4.2. Laser stimulated recombination

The production of ground state antihydrogen atoms is an essential step to achieve high precision spectroscopy. Equally important is to develop a technique to control the quantum states of the $\overline{H}$ atoms. Our laser-induced formation runs were motivated by the possibility to address these issues.

During the 2004 data taking the experimental apparatus was modified to allow the insertion of laser light into the mixing trap to stimulate the radiative formation of antihydrogen in the $n = 11$ quantum state. A CO_2 continuous wave laser was used with a tunable wavelength $9.5 < \lambda < 11.2$ μm; most of the data (345 runs) have been collected

with $\lambda = 10.96\ \mu$m.

The beam waist in the mixing region was about 2 mm with a typical peak intensity of 160 W cm^{-2} at 10 W power. The expected stimulated formation rate with a power of 100 W/cm^2, 10^4 antiprotons and a 10^8 cm^{-3} positron plasma density, was 60 Hz under equilibrium conditions at 15 K.

The spatial overlap of the laser and the positron cloud had been assured through the tight mechanical constraints on the laser beam. With the typical laser waist of 2 mm at the mixing region, the parallel movement of the laser beam was constrained mechanically to ± 1.2 mm in both the horizontal and vertical degrees of freedom.

The physical overlap of laser and positrons was assured by optimizing the laser power transmitted through the apparatus. In order to verify the overlap and check for misalignment, a series of measurements were carried out with the laser shifted ± 1 mm both horizontally and vertically. All these checks have continuously assured good alignment throughout all the laser runs.

Since the transition is from the continuum, the recombination rate is not affected by the finite Doppler width for T = 15 K nor by the laser bandwidth (100 MHz), because the level population and oscillator strength are nearly constant within these widths.

In a steady state situation, the recombination rate is given by [21]

$$R(E)_{n,l} = n_{\bar{p}} N(E) \frac{r^{\mathrm{abs}}_{n,l}(E)\ \gamma_{n,l}}{r^{\mathrm{abs}}_{n,l}(E) + \gamma_{n,l}} \tag{1}$$

where E is the positron energy, $N(E)$ the Maxwellian energy distribution, $n_{\bar{p}}$ the number of antiprotons, $r^{\mathrm{abs}}_{n,l}$ the radiation absorption rate and $\gamma_{n,l}$ is the spontaneous radiative decay rate of the level (n,l).

Beside the formation, there is also the possibility of the inverse process, that is the $\overline{H}$ laser ionization. The probability that ionization takes place is proportional to the interaction time τ with the laser. This time depends either on the experimental conditions (laser pulse length, flight time of the formed $\overline{H}$ in the laser light) or on relaxation properties of the final state (lifetime for spontaneous radiative decay of the recombined system to lower levels not influenced by the laser). If we only consider the spontaneous radiative decay of states and assume that the $\overline{H}$ atoms are formed in equilibrium with the 15 K positron plasma (flight time of about 1 μs in the laser light), we find a finite ionization probability with $n = 11,\ldots,40$ in the $D, F, \ldots$ states. For example, for a $\overline{H}$ atom in the $20D$ state (215 kHz radiative decay rate) there is a 22% chance that it will be ionized. One in a 40D state would have a 2.7% chance of being ionized. If the temperature of the formed $\overline{H}$ atoms is higher than the temperature of the positron plasma, as discussed previously and in [20], an interaction time of 100 ns is estimated, resulting in ionization probabilities ten times lower. Therefore, ionization effects are in principle possible, but a quantitative estimation cannot be made without an accurate knowledge of the $\overline{H}$ velocity and quantum state distributions.

We now consider our laser experimental data from the 2004 runs.

With the laser light into the mixing region (laser ON), no significant increase in temperature and base vacuum deterioration have been measured. However, to assure the same environment conditions between laser OFF and laser ON cold mixings, compari-

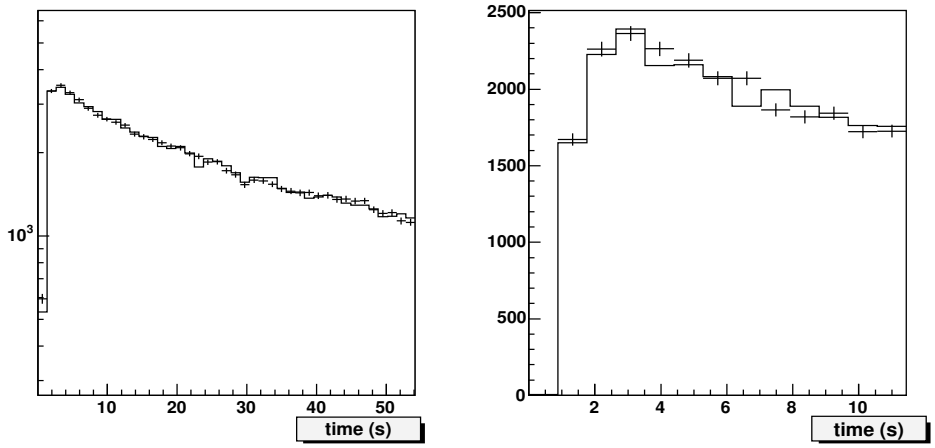

Figure 9. Left: vertex time distribution (log scale) for laser OFF (line) and laser ON (crosses); right: the same for the first 10 seconds in decimal scale.

son was made in the same mixing cycle, by chopping the laser beam at a frequency of 25 Hz, with triggers recorded by the DAQ.

In this way we collected 156160 annihilation events in 345 cold mix runs having a duration of 50 s. By applying the technique of signal plus background fit to the vertex spatial distributions previously used in [8], we find an $\overline{H}$ production percentage of $(55 \pm 4)\%$. The slight decrease with respect to the past $\overline{H}$ production percentage (see Tab. 1) is due to a slight deterioration of the vacuum conditions in the new set-up modified for the laser experimentation. Taking into account the efficiencies, in total we produced about $7\,10^5$ $\overline{H}$, with a mean rate of 40 Hz and a yield of $(20 \pm 4)\%$. The vertex time distribution of all these run is presented in Fig. 9. The curve can be fitted with two exponentials, (not shown in the figure) having time constants of 5.8 s and 52 s respectively. This time behaviour is characteristic of our Penning trap, where different cooling mechanisms are present [15].

In fig. 10 we show the laser ON-laser OFF radial density of vertices and opening angle distributions. The vertex resolution is the same as in Fig. 2.

From these results it is clear that the laser effects are negligible.

This conclusion does not depend on different time or spatial cuts on the vertices and angle distributions. To be more quantitative, we consider the number of vertices in the whole time window of $1 < t < 50$ s and in the intervals $1 < t < 7$ s and $7 < t < 50$ s, corresponding to the two time components present in our data (the results are insensitive to small variations of the widths of these intervals).

In this analysis we use also a subsample of particularly well reconstructed vertices, using the quality index from the vertex algorithm; since this index is calculated on the basis of statistical estimators and of the agreement between different vertex determination methods, the vertex quality selection does not create biases on the physics analysis [6].

The results, for the number of vertices in the interval $0.7 < r < 2.5$ cm (see Fig. 10) are reported in Tab. 2. Although this cut tends to suppress the background, because it

Table 2. number of vertices between the arrows of fig.10 for different time windows.

laser	vertex quality	$1 < t < 50$ s	$1 < t < 7$ s	$7 < t < 50$ s
OFF	NO	59611	11541	48070
	YES	35039	6745	28294
ON	NO	59496	11806	47690
	YES	34731	6987	27744

selects annihilations on the trap wall, similar results are obtained also with no radial cuts. The small effects that we observe from Tab. 2 are a 2.1σ enhancement in favour of laser ON events in the time interval $1 < t < 7$ and a 2.3σ deficit of laser ON events in the interval $7 < t < 50$ s (vertex quality applied). The 90% CL upper limits are 5.6% for the enhancement (corresponding to 2.2 $\overline{H}/s$) and -3.1% for the deficit (corresponding to 1.2 ionized $\overline{H}/s$). The blind result, in the whole time interval $1 < t < 50$ and without vertex quality, gives a 90% CL upper limit for laser enhancement of 0.5%, coresponding to 0.2 $\overline{H}/s$, much lower of the upper limit of 60 $\overline{H}/s$, obtained by assuming a complete overlap between positrons and $\overline{p}$.

This analysis indicates that the laser has no significant effects on the number of reconstructed $\overline{H}$ annihilation vertices. No improvement in the statistical significance of the results is obtained by analysing the opening angle distributions, since the vertex statistics are lower in this case.

We also did 50 runs with the laser detuned to $\lambda = 10.16\ \mu m$ and $\lambda = 11.03\ \mu m$, in some cases heating the plasma to suppress the three-body formation. No significant variations have been observed.

The reasons for the negligible laser effects may be a smaller number of overlapping

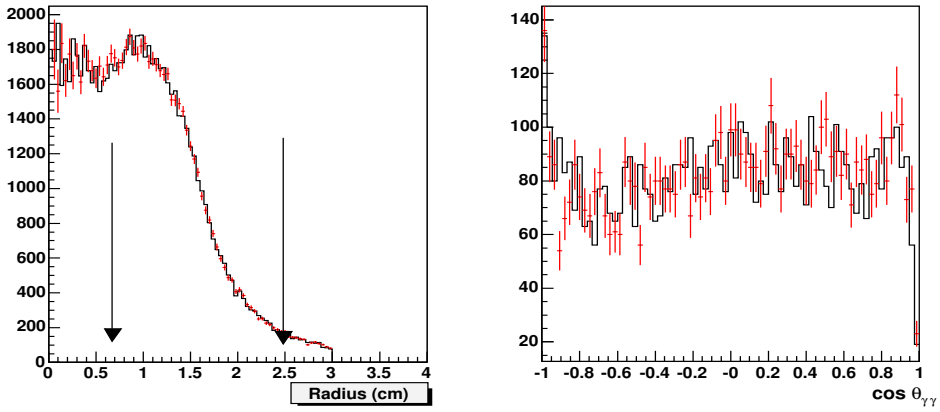

Figure 10. Left: radial vertex distribution for laser OFF (line) and laser ON (crosses). The arrows indicate the zone considered in Tab. 2; right: the same for the opening angle distribution.

antiprotons and/or a higher $\overline{H}$ temperature. In addition, it is likely that the radiative formation in condition of thermal equilibrium is not the dominant $\overline{H}$ formation process; it is therefore possible that, during the positron cooling of the antiprotons, the antiprotons that could participate in the laser induced formation would be "captured" by another competing process (as the three-body collisional formation) at higher temperature. This scenario is consistent with our previous results, reported in sect. 3 and in [11, 20].

4.3. Protonium production

Here we investigate the nature of our background; i.e. of the annihilation events in the trap center.

In Fig.11 the distribution of the radius r (i.e. the distance from the central z axis of the apparatus) versus the longitudinal coordinate z is shown. The data come from the 2003 runs (the center of the trap is at $z \simeq 0.45$ cm) and the reconstructed vertices are affected by uncertainties of σ_z=1.8 mm and $\sigma_x = \sigma_y$=3.5 mm. The background events are clearly displayed for $r < 0.8$ cm, as the discussion below will show.

Fig.11a is for the so called "cold mixing" condition: approximately 10^4 $\bar{p}$ are injected with an energy of about 30 eV into a spheroidal cloud of $\sim 3.5\,10^7$ e^+ previously cooled to the ambient temperature of about 15 K. Fig.11b refers to the so called "hot mixing" where the e^+ are maintained at a temperature of about 8000 K through radio frequency heating of their axial motion.

The two r-z scatter plots look very different: besides the annihilations on the trap surface at r = 1.25 cm there is a component of events localized at small radii which appears in a clear way in cold mixing (Fig.11a), and is dominant in hot mixing (Fig.11b). Looking at the Fig.11a, the radial density distributions in the cold mixing at small radii ($r \leq 0.5$ cm) in the three z-coordinate regions (-1 cm$<z<$0 cm, 0 cm$<z<$1 cm, 1 cm$<z<$2 cm) look very different with opposite behaviour in the central green and lateral blue z-regions.

In Fig.12 the radial distribution of the annihilations is plotted for the hot mixing sample. Most of the events appear in the central region and from Fig.11b we can see that the slope resembles the one in cold mixing sample for $r \leq 0.5$ cm in the central region. The z–coordinate distribution for annihilations with radius less than 0.5 cm is much wider than for cold mixing, see Fig.11.

The examination of the distributions of $\cos\theta_{\gamma\gamma}$ indicates that the events occurring in this region are not $\overline{H}$ annihilations, except for a small fraction in cold mixing due to $\overline{H}$ annihilations on the trap wall that are badly reconstructed. No $\overline{H}$ annihilations occur on the wall for the hot mixing sample. Moreover, the $\cos\theta_{\gamma\gamma}$ distributions for cold mixing in the three z–regions in Fig.11a show that the fraction of non-$\overline{H}$ annihilations on the wall in the central z–region is insignificant.

The distributions in Figs.11 in particular indicate: (1) the observed annihilations are spread in a very different way inside the trap in cold mixing and hot mixing (Figs.11a and Figs.11b); (2) in hot mixing a small fraction of the particles annihilates on the trap wall, and in this case the annihilations do not happen in specific region ('hot spots'), but resemble the $\overline{H}$ distributions.

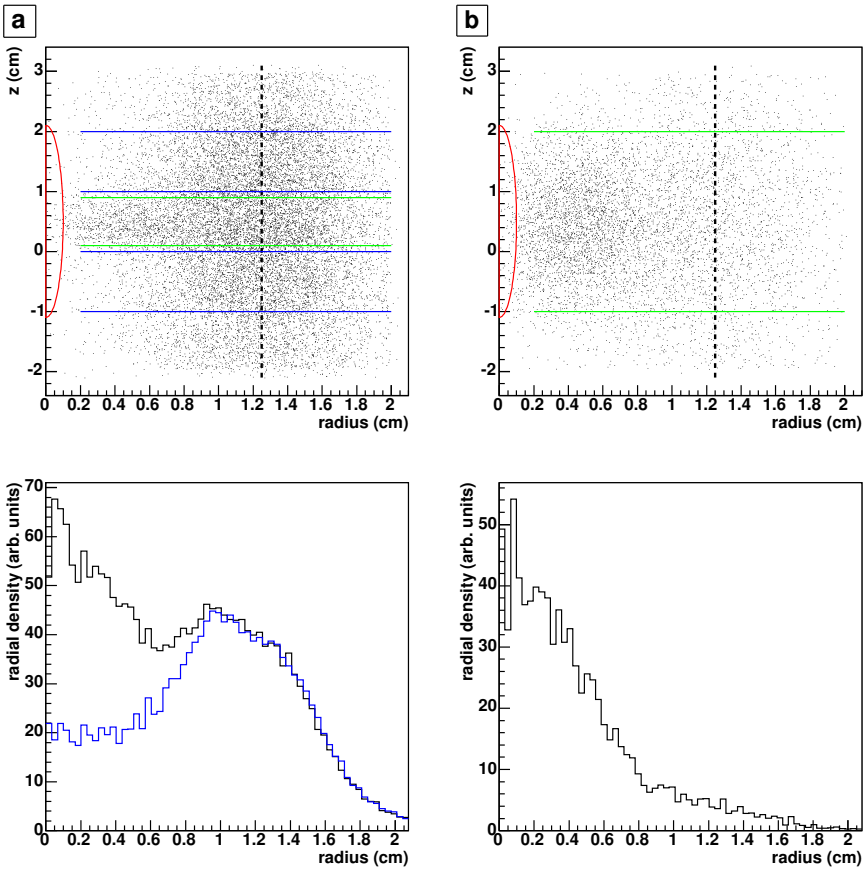

Figure 11. (Color online) *r*-*z* scatter plot and radial densities of the annihilation vertices for: (a) cold mixing; (b) hot mixing. The dashed black line indicates the position of the trap wall; the red semi-ellipse shows the section of the spheroidal e^+ plasma. The black radial densities are for the corresponding central z-region events (inside the green lines) while the blue one is for the the 2 lateral z-regions events, normalized for $r > 1.25$ cm.

Table 3. Experimental and Monte Carlo results concerning the number of tracks due to $\bar{p}$ annihilations.

Data set	Ratio R_{23} on wall	Ratio R_{23} at centre
Cold mixing	1.35±0.01	1.22±0.04
Hot mixing	1.38±0.10	1.17±0.04
$\bar{p}$s only	1.40±0.03	
Monte Carlo $\bar{p}p$	1.19±0.01	1.19±0.01

These features put strong constraints on the formation dynamics and on the particles involved. We cannot assume "direct" annihilations on the confined ions (such as for example $\bar{p}$ annihilations in flight on the ions) since it contradicts the points (1) and (2). Moreover, points (1) and (2) also exclude the possibility that the annihilating systems are charged (as, e.g., for He^{++}) or become charged (as, e.g., for He^+ where the 2nd electron is rapidly ejected).

In addition, the limited z–coordinate values of the annihilation vertices indicate that $\bar{p}$ do not annihilate on neutral residual gas, which is expected to be diffused along the whole trap, as distinct from the ions which are trapped in the central part of the apparatus. At the residual gas pressure of $\sim 10^{-10}$ Pa and at the temperature of ~ 15 K we have counted $10^4 \div 10^5$ ions.

We recall that in another experiment [25] positive ions were produced via ionization of residual gases during injection of the electron beam in a multiring trap. The ion species in the e^+ and ions traps have been identified to be H_2^+ by monitoring the longitudinal oscillation excited by a pulsed RF field. The total number of ions was typically $\sim 10^8$ for electron injection of 30 s and a beam current of 1 μA. This result fits well with ours taking into account the differences in the residual gas pressure, time intervals, electron beam current and so on. Moreover, thanks to the detector granularity we have analyzed the multiplicity pattern of the charged pions emitted from the annihilations, in order to get information about the annihilation processes.

In Tab.3 we report the ratios R_{23} between the number of the reconstructed annihilation vertices having two tracks and the ones with three tracks, for the different data samples and for the central and lateral regions of the trap. We see that the ratio values on the trap wall (2nd column) for all the samples (cold mixing, hot mixing, antiprotons only) are statistically equal as are the ratio values for cold mixing and hot mixing at the trap centre (3rd column). However, the two samples differ by 4 standard deviations, indicating different annihilation mechanisms. Finally, in the last row of Tab.3, the Monte Carlo results (that are obtained assuming $\bar{p}p$ annihilations) are in agreement with the experimental data at the trap center.

To reproduce the main features of the data we assume a model where an $\overline{p}$ in thermal equilibrium with the e^+ plasma can be captured by an (H_2^+) ion trapped inside the plasma:

$$\overline{p} + H_2^+ \rightarrow \overline{p}p + H \ . \tag{2}$$

The formed neutral $\overline{p}p$ system (protonium) is not confined by the electromagnetic field and flies away from the centre of the apparatus. Then it can decay in flight or annihilate on the trap wall. According to [26], we have studied the radial overlap between the e^+ and the relatively small number of ions inside the central well of the nested Penning trap. In our experimental conditions we have calculated that the centrifugal potential barrier, assuming ions and e^+ in equilibrium, is of the order of 10 meV. So, for cold mixing conditions, and assuming in thermal equilibrium with the environment cooled to about 15 K, thermal energy of the ions is not enough to allow them to dive into the plasma and they are consequently confined near the "equatorial region" [27]. On the other hand, for hot mixing conditions, where the e^+ plasma is heated at about 8000 K, the thermal energy of the ions is much higher than the centrifugal barrier, and we can assume that ions are uniformly distributed inside the plasma spheroid.

The velocity of the protonium has been generated using a Maxwellian distribution with the addition of a tangential velocity induced from the rotation caused by the guiding center drift motion, $v_{tang} = \omega r$, where $\omega = \vec{E} \times \vec{B}/|B|^2$. We used the plasma parameters measured by means of the non-destructive technique described in [12, 13].

For the cold mixing case we have generated protonium in a region with a fixed radial position at r_p=1 mm and with a Gaussian distribution along the z-coordinate centered at

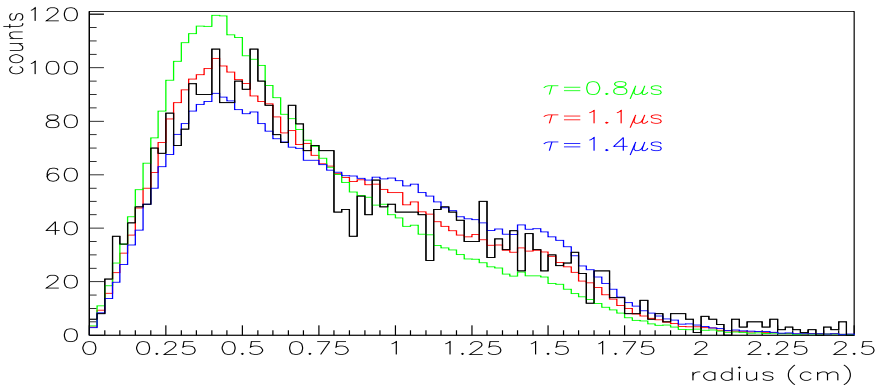

Figure 12. (Color online) Experimental radial distribution of $\bar{p}$ annihilation vertices for hot mixing ($-1 < z < 2$) with Monte Carlo simulation (T=8000 K, $v_{th,mean,x}$ = 5600 m/s, generation inside a spheroid with z_p= 1.6 cm and r_p = 1 mm rotating with f = 300 kHz, i.e. v_{surf}=2000 m/s). Results of simulations with different mean lifetimes are shown: green, τ= 0.8 μs ($\chi^2_{red} = 2.78$); red, τ= 1.1 μs ($\chi^2_{red} = 1.48$); blue, τ= 1.4 μs ($\chi^2_{red} = 2.14$)

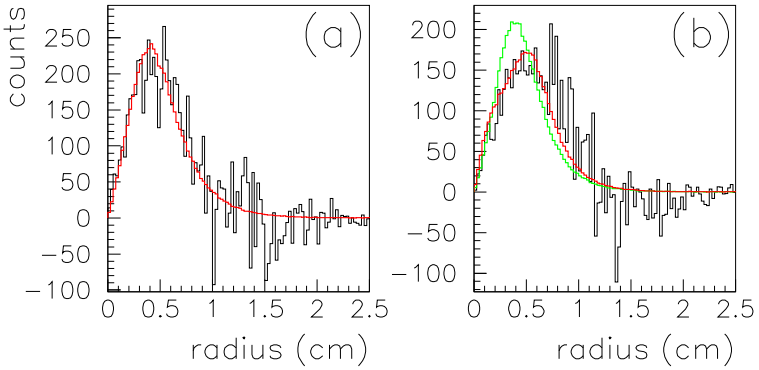

Figure 13. (Color online) Experimental radial distribution for cold mixing 2003 (a) and cold mixing 2002 (b), obtained subtracting the $\overline{H}$ contribution (see text). The red lines are the simulation results (in (a): T=15 K, $v_{th,mean,x}$ = 250 m/s, generation near the equatorial circumference of a spheroid with z_p= 1.6 and r_p = 1 mm rotating with f = 300 kHz, i.e. v_{surf}=2000 m/s; mean lifetime is τ= 1.1 μs; in (b): same parameters as in (a) except for the radius of the spheroid r_p = 2.5 mm and the rotation frequency f = 80 kHz, i.e. v_{surf}=1300 m/s (from 2002 plasma diagnostics). In (b) the green line corresponding to the parameters of the red line in (a) (plasma parameters of 2003) is shown for comparison.

the symmetry plane of the system with σ = 0.25 cm, corresponding to the best fit to the data; for the hot mixing case we have generated protonium with uniform density inside the spheroid, that was characterized by a radius of r_p=1 mm and an axial half-length z_p=16 mm.

Following this prescription, the radial kinetic energy of the formed system results about 1 meV in the cold mixing case and about 700 meV in the hot mixing case. We assume an exponential decay law for the lifetime distribution of the formed system. The mean lifetime of the protonium has been determined by the best fit of the simulations to the real data.

Firstly we discuss the simulations for the hot mixing sample. In Fig.12 the experimental radial distribution is compared to some simulated distributions for different protonium lifetimes. The sensitivity in determining the lifetime is evident, with the best result of $(1.1 \pm 0.1)\ \mu$s.

To analyze the cold mixing sample, we extract the non-$\overline{H}$ annihilations in the central z–region near the center of the trap by subtracting the radial distributions, observed in Fig.11a for the two "blue" lateral z-regions, from the "green" central one.

The results are plotted in Fig.13a with the Monte Carlo simulated events assuming the same lifetime obtained in the hot mixing sample, showing good agreement. In this case, according to the simulation, only a minimal fraction ($\sim 0.5\%$) of the formed protonium arrives on the trap surface, confirming our experimental observation.

In our experimental conditions, for the cold and hot mixing samples, we observe around 10^2 protonium annihilations every $\bar{p}$ injection cycle, i.e. one order of magnitude less than the $\overline{H}$ formed in cold mixing.

The protonium lifetimes are found to be equal in the 'cold' and 'hot' samples, within the experimental resolution.

In conclusion we have demonstrated the possibility to produce metastable protonium in a near–vacuum condition. The kinetic energies are in the range $1 \div 700$ meV. The measured lifetime of 1.1 μs is in agreement with the prediction for near–circular states for n $\simeq$ 34, at low $\bar{p}$ energy capture by H_2^+ [28].

5. CONCLUSIONS

Between 2002 and 2004 ATHENA produced more than 2 million anti-atoms, studying in detail the cooling process of antiprotons inside a very dense positron plasma and determining the conditions to routinely maintain an average antiatom formation rate of 20-40 Hz for about a minute.

Many results of importance for future experiments have been obtained, such as:

- the determination of $\overline{H}$ production rates and yields as a function of some standard mixing conditions [3, 8];
- the observation, for the first time, of the distribution of the particle loss in a Penning trap by reconstructing the annihilation vertices from the trajectories of the charged annihilation products [6, 9];
- the study of the time evolution of the $\overline{p}$ cooling process, with the identification of several distinct types of behaviour [15];
- the dependence of the $\overline{H}$ formation on the temperature and shape of the positron plasma [11, 12, 13, 14];
- the spatial distribution of the antihydrogen atoms leaving the potential well of the trap, and the determination of the $\overline{H}$ axial temperature [20].

Here we also reported on

- some techniques of $\overline{p}$ cooling [22];
- the use of a laser to induce the formation of antihydrogen atoms with principal quantum number n=11;

- the analysis of our background in terms of a protonium formation model.

These results will be object of forthcoming publications.

Since our data suggest that the two-body recombination could not be the main mechanism responsible for the antihydrogen formation, it is likely that many antihydrogen atoms are produced in weakly bound states. How to determine the distribution of these states and to drive the antiatoms to more deeply bound states suitable for spectroscopy are the open challenges for the next generation experiments.

ACKNOWLEDGMENTS

We thank the CERN AD team for assistance and their continuous efforts to assure the best antiproton beam during all the ATHENA runs.

REFERENCES

1. G. Baur *et al.*, *Phys. Lett. B* **368**(1996)251.
2. G. Blanford *et al.*, *Phys. Rev. Lett.* **80**(1998)3037.
3. M. Amoretti *et al.*, ATHENA Collaboration, *Nature* **419**(2002)456.
4. G. Gabrielse *et al.*, *Phys. Rev. Lett.* **89**(2002)213401.
5. G. Gabrielse *et al.*, *Phys. Lett. A* **129**(1988)38.
6. M. Amoretti *et al.*, ATHENA Collaboration, *Nucl. Instr. and Meth. A* **518**(2004)679.
7. C. Regenfus, *Nucl. Instr. and Meth. A* **501**(2003)65.
8. M. Amoretti *et al.*,ATHENA Collaboration, *Phys. Lett. B* **578**(2004)23.
9. M. Fujiwara *et al.*, ATHENA Collaboration, *Phys. Rev. Lett.* **92**(2004)065005.
10. M. Amoretti *et al.*, ATHENA Collaboration, Memorandum to the SPSC: *Progress Report on the ATHENA experiment*, CERN, Geneva (2004).
11. M. Amoretti *et al.*, ATHENA Collaboration, *Phys. Lett. B* **583**(2004)59.
12. M. Amoretti *et al.*, ATHENA Collaboration, *Phys. Rev. Lett.* **91**(2003)055001.
13. M. Amoretti *et al.*, ATHENA Collaboration, *Phys. Plasmas* **10**(2003)3056.
14. L.V. Jørgensen *et al.*, ATHENA Collaboration, *Phys. Rev. Lett.* **95**(2005)025002.
15. M. Amoretti *et al.*, ATHENA Collaboration, *Phys. Lett. B* **590**(2004)133.
16. A. Müller and A. Wolf, *Hyp. Int.* **109**(1997)233.
17. F. Robicheaux, *Phys. Rev. A* **70**(2004)022510.
18. J. Stevefelt, J. Boulmer and J-F. Delpech, *Phys. Rev. A* **12**(1975)1246.
19. P.O. Fedichev, *Phys. Lett. A* **226**(1997)289.
20. N. Madsen *et al.*, ATHENA Collaboration, *Phys. Rev. Lett.* **94**(2005)03403.
21. A. Wolf, *Hyp. Int.* **76**(1993)189.
22. A. Kellerbauer et al., ATHENA Collaboration, submitted to *Phys. Rev. A*.
23. L. S. Brown and G. Gabrielse, *Rev. Mod. Phys.* **58**(1986)233.
24. G. Savard et al., *Phys. Lett. A* **158**(1991)247.
25. N. Oshima *et al.*, Phys. Rev. Lett. **93**(2004)195001.
26. D. H. E. Dubin and T. M. O'Neil, *Rev. Mod. Phys.* **71**(1999)87.
27. T. M. O'Neil, *Phys. Fluids* **24**(1981)1447.
28. K. Sakimoto, *Phys. Rev* A **69**(2004)042710.